# Phase-amplitude coupling of ripple activities during seizure evolution with theta phase

Hiroaki Hashimoto. M.D., Ph.D.[1,2,3]*, Hui Ming Khoo. M.D., Ph.D.[4], Takufumi Yanagisawa. M.D., Ph.D.[4], Naoki Tani. M.D., Ph.D.[4], Satoru Oshino. M.D., Ph.D.[4], Haruhiko Kishima. M.D., Ph.D.[4], Masayuki Hirata. M.D., Ph.D.[1,3,4]

[1] Department of Neurological Diagnosis and Restoration, Graduate School of Medicine, Osaka University, Suita 565-0871, Japan
[2] Department of Neurosurgery, Otemae Hospital, Osaka, 540-0008, Japan
[3] Endowed Research Department of Clinical Neuroengineering, Global Center for Medical Engineering and Informatics, Osaka University, Suita 565-0871, Japan
[4] Department of Neurosurgery, Graduate School of Medicine, Osaka University, Suita 565-0871, Japan

*** Correspondence:**
Hiroaki Hashimoto, M.D., Ph.D.
Invited Researcher, Department of Neurological Diagnosis and Restoration, Graduate School of Medicine, Osaka University, Yamadaoka 2-2, Suita, Osaka, Japan
Tel.: +81-6-6210-8429
Fax: +81-6-6210-8430
E-mail: h-hashimoto@ndr.med.osaka-u.ac.jp

**Key Words:** Seizures; Phase-amplitude coupling; Theta band; Visualization; High-frequency activities; Intracranial EEG;

## Highlights

- We visualized the phase-amplitude coupling phenomenon related to seizures by showing rhythmic fluctuation of high-frequency activities.
- The low frequency band mainly coupled ictal-ripple activities was the θ band (4–8 Hz).

- The seizure-related ripple power started to increase, and then spread, with fluctuations, and not with linear increases.


## Abstract

**Objective**

High-frequency activities (HFAs) and phase-amplitude coupling (PAC) are key neurophysiological biomarkers for studying human epilepsy. We aimed to clarify and visualize how HFAs are modulated by the phase of low-frequency bands during seizures.

**Methods**

We used intracranial electrodes to record seizures of focal epilepsy (12 focal-to-bilateral tonic-clonic seizures and three focal-aware seizures in seven patients). The synchronization index, representing PAC, was used to analyze the coupling between the amplitude of ripples (80–250 Hz) and the phase of lower frequencies. We created a video in which the intracranial electrode contacts were scaled linearly to the power changes of ripple.

**Results**

The main low frequency band modulating ictal-ripple activities was the θ band (4–8 Hz), and after completion of ictal-ripple burst, δ (1–4 Hz)-ripple PAC occurred. The ripple power increased simultaneously with rhythmic fluctuations from the seizure onset zone, and spread to other regions.

**Conclusions**

Ripple activities during seizure evolution were modulated by the θ phase. The PAC phenomenon was visualized as rhythmic fluctuations.

**Significance**

Ripple power associated with seizure evolution increased and spread with fluctuations. The θ oscillations related to the fluctuations might represent the common neurophysiological processing involved in seizure generation.

*Abbreviations:*

CT, Computerized tomography; EEG, Electroencephalograms; FAS, Focal aware seizure; FBTCS, Focal to bilateral tonic-clonic seizures; FIAS, Focal impaired awareness seizure; FLAIR, Fluid-attenuated inversion recovery; FWE, Familywise error; HFAs, High-frequency activities; HFOs, High frequency oscillations; iEEG, Intracranial electroencephalograms; MRI, Magnetic resonance imaging; MTL, Mesial temporal lobe; P, Patient; PAC, Phase-amplitude coupling; PRC, Preceding ripple contact; S, Seizure; SD, Standard deviation; SI, Synchronization index; SIm, Synchronization index magnitude; SImb, Bootstrapping synchronization index magnitude; SO, Seizure onset; SOC, Seizure onset contact; SOZ, Seizure onset zone; 3D, Three-dimensional;

## 1. Introduction

Intracranial electroencephalograms (iEEG) allow acquisition of wideband waveforms, from slow shift to high-frequency activities (HFAs), at a high signal-to-noise ratio. Direct current (DC) shifts and infraslow activities, which are very slow-frequency components, appear in the seizure onset zone (SOZ) during a seizure (Ikeda et al., 1999, Imamura et al., 2011, Kanazawa et al., 2015, Rodin and Modur, 2008). HFAs can be physiological, i.e., those recorded during a task (Hashimoto et al., 2017, Hashimoto et al., Hashimoto et al., 2020b), or pathological, i.e., those observed during seizures or interictal period in epileptic patients (Akiyama et al., 2006, Imamura et al., 2011, Zijlmans et al., 2012). High frequency oscillations (HFOs) are subgroup of HFAs and isolated oscillations standing out from the background, within the high frequency range usually above 80 Hz. Ictal HFOs occur in the SOZ (Jirsch et al., 2006, Modur et al., 2011), and HFOs can be further classified into ripples (80–250 Hz) and fast ripples (250–500 Hz) (Modur et al., 2011). Previous study reported that HFAs were useful for detection of seizures(Ayoubian et al., 2013).

The amplitude of HFAs is modulated by the low-frequency oscillation phase (Canolty et al., 2006). Physiologically, this phase-amplitude coupling (PAC) has various functional roles in cortical processing such as motor execution (Yanagisawa et al., 2012) and sensory processing (Luo and Poeppel, 2007). In the ictal state, PAC achieved high values in the SOZ (Ibrahim et al., 2014, Iimura et al., 2018). Moreover, it is reported that PAC between the infraslow phase and HFAs amplitude preceded the seizure onset (SO) (Hashimoto et al., 2020a).

PAC achieves high values in the SOZ during seizures; however, there is no consensus about the main low frequency band that modulates the amplitude of HFAs. Several low frequency bands have been reported like δ (Iimura et al., 2018, Nariai et al., 2011, Nonoda et al., 2016), θ (Ibrahim et al., 2014), α (Ibrahim et al., 2014), and β (Edakawa et al., 2016) bands.

Furthermore, whereas dynamic HFAs changes in the ictal state have been visualized using topographic videos (Akiyama et al., 2006), dynamic PAC changes have not been visualized. The purpose of this study is twofold. One is to clearly identify the main low frequency band contributing to PAC during seizures. The other is to visualize the PAC phenomenon. Using the iEEG, we collected data from 15 seizures in seven patients with medically refractory focal epilepsy. Twelve focal-to-bilateral tonic-clonic seizures (FBTCS), and three focal-aware seizures (FAS) were investigated. First, we evaluated dynamic changes and characteristics of PAC from pre-ictal to late-ictal. Next, we created a video for each patient in which circles, corresponding to electrodes, change their diameters that correlate linearly with the power of HFAs represented by ripples (Video 1–3). We hypothesized that PAC can be visualized using dynamic ripple power changes modulated by a low-frequency band.

## 2. Materials and Methods

### *2.1. Subjects*

We enrolled patients with drug-resistant focal epilepsy who underwent intracranial electrodes placement for presurgical invasive electroencephalograms (EEG) study who were admitted to Osaka University Hospital from July 2018 to July 2019. This retrospective study was approved by the Ethics Committee of Osaka University Hospital (Suita, Japan) (approval no., 19193). Informed consent was obtained by the opt-out method on our center's website.

### *2.2. Intracranial electrodes and their location*

Data on iEEG were acquired using a combination of subdural grids (10, 20, or 30 contacts), strips (four or six contacts), and depth electrodes (six contacts) (Unique Medical Co. Ltd., Tokyo, Japan), placed using conventional craniotomy. The diameter of each contact was

3 or 5 mm, and the inter-contact distance was 5, 7, or 10 mm for grid and strip electrodes. The diameter was 1.5 mm, and the inter-contact distance was 5 mm for depth electrodes. Three-dimensional (3D) brain renderings were created using FreeSurfer (https://surfer.nmr.mgh.harvard.edu) with the preoperative magnetic resonance imaging (MRI) images. Using Brainstorm (http://neuroimage.usc.edu/brainstorm/), the post-implantation computerized tomography (CT) images were overlaid onto the 3D brain renderings to obtain the position of contact for each electrode in the Montreal Neurological Institute coordinates system.

### *2.3. Data acquisition and preprocessing*

Signals from the iEEG were acquired at a sampling rate of 1 kHz and a time constant of 10 s, using a 128-channel digital EEG system (EEG 2000; Nihon Kohden Corporation, Tokyo, Japan). The raw signals were then preprocessed using a low-pass filter at 333 Hz (to prevent aliasing) and a 60-Hz notch filter (to eliminate the alternating current line artifact) using the BESA Research 6.0 software (BESA GmbH, Grafelfing, Germany). Artifactual signals from electrodes were excluded from further analyses. For the purpose of signal analysis, iEEG signal of each electrode contact was digitally re-referenced to a common average of all electrode contacts in each patient.

All the subsequent signal analysis was performed using MATLAB R2019b (MathWorks, Natick, MA, USA). Our iEEG data were saved every 60 min and thus each iEEG dataset contains a 60-min signal. A bandpass filter using a two-way least-squares finite impulse response filter (pop_eegfiltnew.m from the EEGLAB toolbox, https://sccn.ucsd.edu/eeglab/index.php) was applied to the preprocessed signals of the whole 60-min data to prevent edge-effect artifacts, before we extract iEEG segments for subsequent signal analysis.

### *2.4. Seizure onset contact (SOC)*

The SO were determined by visual inspections of iEEG signals using low-voltage fast activity (Perucca et al., 2014), disappearance of the background activity (Ikeda et al., 1999), and DC shifts (Ikeda et al., 1996) et al. We defined the SOC as contacts that showed initial epileptic iEEG changes. If one patient with more than one seizure exhibited several SOC which fulfilled the condition, and the contacts were commonly involved at seizure onset across all seizures, then we randomly selected one contact in order to simplify the analysis (Fig. 1A).

### *2.5. High frequency activity power changes*

We analyzed the iEEG data acquired 5 minutes before and after the SO for each recorded seizure. We used the ripple band (80–250 Hz) to represent HFA. The time series of the HFA power on each contact was constructed every second from the preprocessed iEEG signal by using a band-pass filter (80–250 Hz) in combination with the Hilbert transformation (Cohen, 2008). The HFA power was then normalized by dividing the power at each second by the average HFA power of the initial 60 s.

### *2.6. Preceding ripple contact (PRC)*

*Preceding* ripple activities were observed as a cluster after the SO if the ripple normalized power exceeded 10, continued for more than a few seconds, and preceded the later ripple activities. We defined contacts that showed the preceding ripple activities as PRC (Fig. 1B). Moreover, we investigated whether the SOC matched the PRC (SOC-PRC concordance; Table 1).

### *2.7. PAC analyses*

We used synchronization index (SI) (Cohen, 2008) to measure the strength of cross-frequency coupling between the amplitude of ripple and the phases of lower frequency bands,

which include δ (1–4 Hz), θ (4–8 Hz), α (8–13 Hz), and β (13–30 Hz).

Hilbert transformation was performed on the bandpass filtered signals to obtain the complex-valued analytic signals of each frequency band, $Z_\omega(t)$ (ω means the frequency band). For each frequency band, the amplitude, $A_\omega(t)$, and phase, $\varphi_\omega(t)$, were calculated from the complex-valued signals using Equation 1.

$$Z_\omega(t) = A_\omega(t) \cdot \exp\left(i\,\phi_\omega(t)\right) \quad (1)$$

The phase of each lower frequency band, $\varphi_l(t)$, was obtained from the angle of the Hilbert transform of the bandpass filtered signal.

To obtain the surrogate signal that represent the time series of the ripple band amplitude, the amplitude of ripple band was first extracted using the squared magnitude of $Z_\gamma(t)$, the analytic signal calculated using the Hilbert transformation ($P_\gamma(t)$ = real $[Z_\gamma(t)]^2$ + image $[Z_\gamma(t)]^2$); then the phase of this amplitude was computed using Hilbert transformation ($\varphi_\gamma(t)$ = arctan (image $[Z(P_\gamma(t))]$/real$[Z(P_\gamma(t))]$)).

SI was calculated using Equation 2.

$$SI = \frac{1}{n} \times \sum_{t=1}^{n} e^{i}[\,\phi_l(t) - \phi_\gamma(t)] \quad (2)$$

We calculated SI for every 1-s time window, which sequentially shifted every 33 ms from 5 minutes before to 5 minutes after the SO. n is the number of time points within each 1-s time window. SI is a complex number; therefore, we used the magnitude of SI, referred to as SIm. SIm varies between 0 and 1, with 0 indicating that phases are completely desynchronized and 1 indicating that phases are perfectly synchronized.

### *2.8. Correlation analysis related to PAC*

We analyzed the correlation between SIm and ripple normalized power in the following three states in relation to seizure onset: pre-ictal (from -1.5 to 0 min before the SO), ictal (from 0 to 1.5 min after the SO), and late-ictal (from 1.5 to 3.0 min after the SO) states

using implanted all contacts (total 1189 electrode contacts). Pearson correlation coefficients were calculated.

### *2.9. Phase-conditioned analysis*

To identify the lower frequency phase to which ripple power was coupled, we computed the average oscillation of each lower frequency band on the SOC across all seizures (15 seizures) and the average ripple normalized power on the SOC. The phases of δ and θ band, were divided into 12 intervals of 30° without overlaps: 0° ± 15°, 30° ± 15°, …, 300° ± 15°, and 330° ± 15°, resulting in 12 phase bins. The reason for choosing these two bands is described in the result section. For each state (pre-ictal, ictal, and late-ictal), the ripple normalized power on the SOC was averaged within each phase bin. Using signal from the SOC instead of the average of all electrode contacts avoids averaging from obscuring the characteristics-of-interest.

### *2.10. Visualization of synchronized multimodal data*

Multimodal data, including iEEG waveform, ripple normalized power, and SIm, were synchronized and simultaneously displayed. To construct a power distribution map, we calculated the power of ripple using the periodogram. The period of 10 seconds before SO was defined as the baseline, and the baseline ripple power was obtained from the baseline segment. We calculated the ripple power within a 500-ms sequential time window every 33 ms (30 frame per second). The ripple power ratio was calculated by dividing the ripple power of the 500-ms time window with baseline ripple power. We plotted red circles on the brain image to indicate the electrode locations, and the diameters were scaled linearly with ripple power ratio.

### *2.11. Statistics*

The ripple normalized power and SIm values were averaged across all contacts in each seizure, and then averaged ripple normalized power and averaged SIm values were averaged

across all seizures. SIm values were normalized using SIm values calculated from the data acquired five minutes before the SO to allow comparison between different low frequency bands. The values greater than +3 standard deviation (SD) or less than -3 SD were excluded as outliers. We used Wilcoxon signed-rank test for pairwise comparison or Wilcoxon rank-sum test for non-pairwise comparison, and Bonferroni correction for multiple comparisons. To compare the ripple power and SIm to the base period (the initial 10-s data), we used a permutation test (Maris and Oostenveld, 2007) and a familywise error (FWE)-corrected threshold for multiple comparisons. Each permutation test produces a set of differences between the base period and the next sequential period. The maximum value of the differences from each permutation test were stored. The values at 95% of the distribution of these maximum values were taken as the FWE-corrected threshold. The values above the FWE-corrected threshold are statistically significant (Cohen, 2014). For comparison of multiple groups, we used the Kruskal-Wallis test.

To assess the significant change in SIm, we used the boot-strapping technique. First, the phase of ripple power time series was shifted in time by a random amount. Then, this phase-shifted ripple power time series was used to calculate a SIm value for the purpose of bootstrapping (SImb). For each pair of ripple power and a lower frequency band amplitude, this procedure was repeated 1000 times to create the distribution of SImb (Cohen, 2008). To correct for multiple comparisons, we used the FWE-corrected threshold (95%) (Cohen, 2014).

### *2.12. Data availability*

All data that were generated by or analyzed in this study are available from the corresponding authors upon reasonable request and after additional ethics approvals regarding the data provision to individual institutions.

## 3. Results

### *3.1. Profile of ripple power and PAC changes related to seizures*

We included seven patients (six male and one female) with 12 focal impaired awareness seizure (FIAS)/FBTCS and three FAS (Table 1). The pathological results of each patient are shown in Table 1. We compared ripple normalized power between the pre-ictal and the ictal states. The ripple normalized power at the ictal state were significantly larger than at the pre-ictal state (single-sided Wilcoxon signed-rank, $P = 3.1 \times 10^{-5}$) (Fig. 2A). Averaged time of seizures is 125.73 ± 55.1 s, and times of each seizure are shown in Table 1. Among all seizures analyzed, SOC were concordant with PRC in 12/15 seizures (80%). When focusing on only FBTCS, SOC matched PRC in all seizures (Table 1).

We compared SIm values between ripple activity and each lower frequency band during the burst of ripple power at the ictal state. The normalized SIm of ripple-θ was the highest among all (single-sided Wilcoxon signed-rank with Bonferroni correction, θ-δ: corrected $P = 3.0 \times 10^{-3}$, θ-α: corrected $P = 1.3 \times 10^{-2}$, θ-β: corrected $P = 2.3 \times 10^{-3}$) (Fig. 2B). The main low frequency band coupled with ripple was the δ band in 2/15 seizures (13%), θ band in 12/15 seizures (80%), and α band in 1/15 seizures (7%) (Table 1). We investigated the low frequency power at pre-ictal and ictal states; however, the main low frequency band that showed coupling with ripple did not match the low frequency band showing increased power (Supplementary Fig. 1).

### *3.2. Temporal profile of ripple power and PAC changes*

Dynamic changes of ripple normalized power and PAC strength from 5 min before to 5 min after the SO are shown in Fig. 2C. A significant burst of ripple power was observed after the SO, which was accompanied by two different profiles of PAC with the lower frequency bands: (1) PAC changes with a peak (θ-, α-, and β-ripple coupling) and (2) PAC changes with

277 a gradual increase and a plateau (δ-ripple coupling). For those with the first profile, the PAC
278 for θ band after SO were the higher than those for α and β bands, which were also reflected in
279 their differences shown in Fig. 2B. For the second profile, the PAC for δ band increased
280 gradually and reached its maximum after ripple power burst, which was not reflected in the
281 difference shown in Fig. 2B that was obtained from the data during the burst of ripple power
282 within the ictal state. We focused on PAC for θ band (representing the first profile) and δ band
283 (the second profile) in the following analyses.
284
285 *3.3. Case studies*
286 During seizures, the ripple power increased and was coupled with the θ phase. After
287 completion of ripple power burst, δ-ripple coupling occurred. We show the synchronized
288 multimodal data including iEEG waveforms, ripple normalized power, SIm, and ripple power
289 distribution map in the figure and videos of three illustrative cases. In Fig. 3, 4, and 5,
290 significant θ-ripple SIm and representative contacts are shown. In videos (Video 1–3),
291 significant δ- and θ-ripple SIm and all contacts are shown.
292
293 *3.3.1 Case #1; Patient 1 (P1)–Seizure 1 (S1)*
294 Interictal scalp EEG recorded spike-wave complexes over the right temporal region.
295 We placed intracranial electrodes in the right hemisphere (Fig. 3A). MRI images showed a
296 cystic lesion in the right mesial temporal lobe (MTL) (Fig. 3B).
297 We captured electroclinical seizures consisting of FIAS, followed by FBTCS. Contact
298 A2 on the depth electrode inserted in the right parahippocampal gyrus, showed initial DC shifts,
299 followed by low-voltage fast waves that changed into high-amplitude fast waves and spread to
300 the other electrodes (Fig. 3C). Ripple power increases also began from A2 and spread to the
301 other electrodes (Fig. 3D and 3F). A2 is SOC as well as PRC. Significant θ-ripple SIm values
302 were observed in the contacts in which ripple power increased (Fig. 3E), and after that,

significant δ-ripple SIm values were observed (Video 1). Ripple-band power (represented by the size of the red circle) fluctuated rhythmically at certain rhythms when θ-SIm reached statistical significance and this relationship was also observed for δ-band (Video 1).

We resected the right mesial temporal lobe including the cystic lesion and the parahippocampal gyrus. Pathological findings showed the presence of dysembryoplastic neuroepithelial tumor. He was seizure-free at the 12-month follow-up.

*3.3.2 Case #2; P4–S2*

Interictal scalp EEG recorded spike-wave complexes over the left frontotemporal region. We placed intracranial electrodes in the left hemisphere (Fig. 4A). MRI fluid-attenuated inversion recovery (FLAIR) images showed a high-intensity lesion in the left MTL (Fig. 4B).

We captured FIAS, followed by FBTCS. Contact A13 on the depth electrodes, which were inserted in the left mesial temporal lesion, showed initial DC shifts, followed by low-voltage fast waves that changed into high-amplitude fast waves and spread to the other electrodes (Fig 4C). Ripple power increases also began from A13 and propagated to other electrodes (Fig. 4D and 4F). A13 is SOC as well as PRC. Significant θ-ripple SIm values were observed in contacts in which ripple power increased (Fig. 4E), and after that, significant δ-ripple SIm values were observed (Video 2).

We performed a left selective hippocampectomy including the FLAIR high lesion, also removing the amygdala. Pathological findings showed hippocampal sclerosis. She was seizure-free at the 12-month follow-up.

*3.3.3. Case #3; P5–S2*

Interictal scalp EEG recorded spike-wave complexes over the right temporo-occipital region. We placed intracranial electrodes in the right hemisphere (Fig. 5A). MRI FLAIR images showed a high-intensity lesion in the right occipital lobe (Fig. 5B).

We captured electroclinical seizures, followed by bilateral lower extremities stereotypies (FBTCS). The A31, A32, A36 and A37 contacts, which were placed over the occipital lesion, showed initial DC shifts, followed by low-voltage fast waves that changed into high-amplitude fast waves (Fig. 1A, Fig. 5C). Ripple power increases also began from these four contacts and propagated to the other electrodes (Fig. 5D and 5F). SOC-PRC concordance was observed. Significant θ-ripple SIm values started to appear in contacts which were placed over the occipital lesion (Fig. 5E), and after that, significant δ-ripple SIm values were also observed (Video 3).

We performed a resection surgery of the right occipital lesion. Pathological findings showed diffuse glioma. He was seizure-free at the 12-month follow-up.

In all three cases, SOC was concordant with the PRC, and the time lag between θ and δ PAC was observed. Rhythmically fluctuations of ripple activities were visualized in the power distribution map when the values of SIm were significantly high (Video 1, 2, and 3).

### *3.4. Time when the maximum values were observed*

There was no significant difference between the time taken (since SO) to attain maximum ripple power (77.6 ± 38.9 s) and maximum θ PAC (73.7 ± 41.7 s); however, the time taken to achieve maximum value of δ PAC (117.7 ± 70.9 s) was significantly more than that for both ripple power and θ PAC (single-sided Wilcoxon signed-rank with Bonferroni correction, ripple power and δ PAC, corrected $P = 1.6 \times 10^{-3}$, θ PAC and δ PAC, corrected $P = 8.2 \times 10^{-4}$) (Fig. 6A). A time lag between θ and δ PAC was observed in 14/15 seizures (93.3%) (Table 1).

### *3.5. Correlation between ripple normalized power and SIm*

To clarify the differences between PAC for θ and δ bands, correlation analysis was

used. The correlation of ripple with the SIm of θ band was positive in all three states (pre-ictal, ictal and late-ictal), in which a statistical significance was reached in the ictal state. In contrast, the correlation with the SIm of δ band was positive in the pre- and late-ictal states and negative in the ictal state, in which a statistical significance was reached in all three states (Fig. 6B).

### *3.6. Phase-tuning ripple power*

The oscillation of δ and θ bands showed a trough at 180° in all pre-ictal, ictal and late-ictal states (Fig. 6C). In the ictal state, in which θ-SIm increased (Fig. 2C), ripple normalized power peaked at the trough of the θ oscillation but not the δ oscillation (Fig. 6C). In the late-ictal state, in which δ-SIm increased (Fig. 2C), ripple normalized power peaked at the trough of the δ oscillation (Fig. 6C).

### 3.7. Comparison between FBTCS and FAS

In 12 FBTCS in which seizures showed sequential changes from no motor symptom to tonic seizures and finally to clonic seizures, the average dynamic changes in the ripple normalized power were compared at these different ictal phases (Fig. 7A). The ripple normalized power of both tonic and clonic phases was significantly higher than that of the no motor symptom phase; however, there were no significant changes between the tonic and clonic phases (both-sided Wilcoxon rank-sum with Bonferroni correction, no motor-tonic: corrected $P = 1.9 \times 10^{-116}$, tonic-clonic: corrected $P = 1.2$, no motor-clonic: corrected $P = 2.7 \times 10^{-110}$).

Finally, we compared θ-ripple SIm and ripple normalized power acquired from the SOC during the no motor symptom phase between FBTCS and FAS (Fig. 7B). FBTCS showed significantly higher values than FAS in SIm (both-sided Wilcoxon rank-sum, $P = 2.3 \times 10^{-267}$) and ripple normalized power (both-sided Wilcoxon rank-sum, $P = 0$).

## 4. Discussion

This study demonstrated that a ripple power burst occurs during seizures, and the phase of θ band modulates ripple power involved in seizures. Our videos showed that when ripple power increased, the individual ripple power of each contact (corresponded to the size of each red circle in the video) changes rhythmically. During such rhythmic fluctuation in the circles' size, a significant θ-ripple PAC was observed. Therefore, we inferred that the rhythmic fluctuation in the circles' size (in the video) was modulated by the θ rhythm and this fluctuation represented the θ-ripple PAC phenomenon. Our video also showed that in FBTCS, ripple activities involved in seizures started to increase from the focal area and spread to other regions, but with fluctuations and not linearly.

How HFAs were propagated during seizures has been visualized by topographic videos (Akiyama et al., 2011, Akiyama et al., 2006), however, PAC changes involved in seizures have not been visualized. In our videos, the diameters of each circle that represents an implanted electrode contact changed with ripple power, and the videos also demonstrated the propagation of HFAs by dynamic changes of circles' diameters. Moreover, the rhythmic fluctuations of the diameter were observed in each contact. When δ- or θ-ripple PAC significantly increased, the rhythmic fluctuation of the circles' diameter became especially obvious. We inferred that this rhythmic fluctuation of the circles' diameter was tuned at δ- or θ rhythm, and concluded that this rhythmic fluctuation visualized the PAC phenomenon.

HFAs have been observed during seizures (Akiyama et al., 2011, Ochi et al., 2007) and HFOs are suggested as useful biomarkers for detection of the SOZ (Wang et al., 2013, Wu et al., 2014). In this study, significant increase in ripple power was observed during seizures, and PRC which showed preceding ripple activities were demonstrated (Fig. 3D, 4D, and 5D, and videos). The SOC was conventionally determined by visual inspection (Perucca et al., 2014), and we demonstrated that in FBTCS, the SOCs were concordant with the PRCs.

Therefore, we thought that ripple activities were useful for detection of the SOZ.

In FBTCS, the more the seizure progressed, the more the ripple activities increased. The videos in this study showing seizure evolution of FBTCS demonstrated that the focal fluctuations of ripple activities increased and spread to other regions. The results of the videos indicated that ripple activities involved in seizures increased and spread with fluctuations, but not linearly. In clinical situations, our video helped us find the SOZ using focal ripple activities. Moreover, in actual clinical settings, we synchronized the multimodal data (iEEG, ripple normalized power, and SIm) with video images captured by the video-EEG camera; therefore, we could infer the symptomatogenic zone by correlating seizure symptoms captured by video-EEG camera with the spread of ripple activities. In this study, images captured by the video-EEG camera were not presented because of privacy issues.

In line with a previous study (Ibrahim et al., 2014), our study demonstrated that θ band was the main low frequency band modulating ictal-ripple activities and α- and β-ripple PAC showed the same tendency as the θ-ripple PAC with a weaker PAC though. Moreover, it is reported that coupling with θ waves and HFOs well discriminated normal brain regions from SOZ (Amiri et al., 2019). Therefore, we inferred that ripple activities occurring during early seizure evolution were modulated by θ rhythm. The occurrence of maximal ripple power at the trough of the low frequency oscillation was concordant with a previous study(Ibrahim et al., 2014). In an interictal state, a positive correlation between coupling and ripple amplitude were known(Weiss et al., 2016), and we showed the positive correlation between θ-ripple PAC and ripple power during the ictal state.

Previous studies showed that prior to the onset of bilateral tonic-clonic movements, ripple density in the SOZ was higher in FBTCS than in focal seizures (Schönberger et al., 2019).

This result is concordant with our result that in the SOZ, the ripple normalized power was higher in FBTCS than in FAS during the early no motor symptom phase. Moreover, we showed that θ-ripple SIm was also higher in FBTCS than in FAS, which reflected the results of the positive correlation between θ-ripple PAC and ripple power during the ictal state.

The low frequency band that coupled with ripple activities involved in seizures varied in one patient and also between patients; however, in most seizures, the θ band is the main band. Between various pathological results, the main low frequency coupling with ripple activities was the θ band in common. This result might indicate the common neurophysiological processing that neural activities involved in seizure generation and spreading were mainly regulated by the θ rhythm. Animal experiments showed that in the epileptic brain, the hippocampal θ rhythm was increased (Kitchigina and Butuzova, 2009). However, in this study, the sample size was too small to investigate the statistical differences or similarities of each pathology.

A seizure is generated by depolarization and repetitive firing of neurons, and the frequency of epileptic EEG activities have been shown to be involved in the thalamocortical network (Dichter, 1997). HFA power is strongly correlated with neural firing rate (Ray et al., 2008), and in animal studies, neural spiking is locked to the trough of the α oscillations (Haegens et al., 2011). Our results showed that ripple normalized power peaked at the trough of the δ or θ oscillation during coupling occurrences. This result may indicate that repetitive neural firing involve in seizure generation is locked to the trough of the δ or θ oscillations. Furthermore, the neural mechanism for how tonic and clonic seizures are induced in FBTCSs has remained unclear. In all FBTCSs of this study, we observed a time lag between the first occurrence of a θ-ripple coupling and the next occurrence of a δ-ripple coupling. Since a tonic seizure occurred first and then a clonic seizure occurred next in FBTCSs, we hypothesized the

following neurophysiological mechanism in FBTCSs: the thalamus first modulates the cortex at the θ rhythm and then a tonic seizure is induced; next, the thalamus modulates the cortex at the δ rhythm and then a clonic seizure is induced.

We showed finding that δ-ripple PAC had a negative correlation with ripple power during ictal-ripple power burst, and increased after ictal-ripple power burst subsided. Coupling between HFAs and δ band were investigated in previous studies associated with epileptic spasm(Nariai et al., 2011) and an interictal state(Amiri et al., 2016). Our videos brought a new insight that δ-ripple PAC significantly increased after θ-ripple PAC. Our results suggested that δ- and θ-ripple PAC were caused by different mechanisms, and this explained the time lag between δ- and θ-ripple PAC.

This study had some limitations. Because intracranial EEG electrodes covers only a small portion of the brain, we can never be sure if the intracranial electrodes were placed in the actual SOZ, and thus the activities that we analyzed may not be the actual activities from the SOZ. To limit the effect of this uncertainty, we used the average ripple power and SIm from all electrodes because we could evaluate at least seizure-related changes which were propagated activities from the SOZ not focal activities of the SOZ. All the seizures were recorded after an extensive reduction of antiepileptic drugs, and thus, they might not represent the patients' usual seizures. However, our analysis were independent from this issue because reduction in medication does not affect the morphology of discharges at onset, and duration of contralateral spread (So and Gotman, 1990). Because this study included only patients with focal epilepsy, our findings may not be generalized to patients with generalized epilepsy. Moreover, because we had only three seizures of FAS, more FAS cases must be analyzed to confirm the differences between FBTCS and FAS. Finally, our sampling rate of iEEG was 1 kHz; therefore, the available frequency range was limited under 300 Hz, and fast ripples usually corresponding to

250-500/600 Hz could not be analyzed.

## 5.Conclusions

By analyzing seizure evolution of focal epilepsy using ripple power and PAC, this study revealed that θ band is the main low frequency band modulating ripple power during ictal-ripple burst. The video we created demonstrated that ripple powers began to increase focally with fluctuations, and spread with fluctuations, not with linear increases. We concluded that the fluctuations are a visualization of the PAC phenomenon. The θ oscillations might represent the common neurophysiological processing involved in seizure generation.

## Declaration of Competing Interest

The authors declare that they have no known competing financial interests or personal relationships that could have appeared to influence the work reported in this paper.


## Acknowledgements

This study was supported by the Grants-in-Aid for Scientific Research (A) (KAKENHI; grant no., 18H04166) and the Grants-in-Aid for Early-Career Scientists (KAKENHI; grant no., 18K18366), which are funded by the Japan Society for the Promotion of Science (JSPS; Tokyo, Japan).


## Author Contributions

H.H. conceived the study, collected the data, created the MATLAB program, analyzed the data, created all figures and the video, and was primarily responsible for writing the manuscript. H.M.K., N.T., S.O., H.K., and M.H. performed the epileptic surgery. All authors clinically cared for and evaluated the patient. H.M.K., T.Y., and M.H. advised H.H. on scientific matters. H.M.K revised the manuscript. H.K. and M.H. supervised this study. All authors have reviewed the manuscript.

| Patients number | Sex | Laterality | Pathology | Seizure numbers | Seizure type | Seizure duration (s) | Preceding ripple activities | SOC-PRC concordance | Coupling low frequency band | Time lag between δ and θ coupling |
|---|---|---|---|---|---|---|---|---|---|---|
| P1 | Male | Right | MTLE DNT | S1 | FIAS→FBTCS | 154 | Yes | concordant | θ | Yes |
| | | | | S2 | FIAS→FBTCS | 144 | Yes | concordant | θ | Yes |
| | | | | S3 | FIAS→FBTCS | 156 | Yes | concordant | α | Yes |
| | | | | S4 | FIAS→FBTCS | 266 | Yes | concordant | θ | Yes |
| | | | | S5 | FIAS→FBTCS | 184 | Yes | concordant | θ | Yes |
| P2 | Male | Right | PLE Glial-cortical tissue with psammoma body-like lesion | S1 | FIAS→FBTCS | 49 | Yes | concordant | δ | Yes |
| P3 | Male | Left | OLE* | S1 | FIAS→FBTCS | 132 | Yes | concordant | θ | Yes |
| P4 | Female | Left | MTLE, HS | S1 | FIAS→FBTCS | 102 | Yes | concordant | θ | Yes |

| | | | | | | | | | | |
|---|---|---|---|---|---|---|---|---|---|---|
| | | | | S2 | FIAS→FBTCS | 113 | Yes | concordant | θ | Yes |
| P5 | Male | Right | OLE Diffuse glioma | S1 | FIAS→FBTCS | 96 | Yes | concordant | θ | Yes |
| | | | | S2 | FIAS→FBTCS | 81 | Yes | concordant | θ | Yes |
| | | | | S3 | FIAS→FBTCS | 129 | Yes | concordant | θ | Yes |
| P6 | Male | Left | MTLE HS | S1 | FAS | 149 | Yes | discordant | θ | No |
| P7 | Male | Right | MTLE FCD | S1 | FAS | 67 | Yes | discordant | θ | Yes |
| | | | | S2 | FAS | 64 | Yes | discordant | δ | Yes |

**Table 1 Clinical profile.**

DNT, Dysembryoplastic neuroepithelial tumor; FAS, Focal aware seizure; FBTCS, Focal to bilateral tonic-clonic seizure; FCD, Focal cortical dysplasia; FIAS, Focal impaired awareness seizure; HFAs, High-frequency activities; HS, Hippocampal sclerosis; MTLE, Mesial temporal lobe epilepsy; OLE, Occipital lobe epilepsy; PLE, Parietal lobe epilepsy; PRC, Preceding ripple contact; SOC, Seizure onset contact;

*Focal resection surgery had not been performed because the detection of the seizure onset zone was impossible.

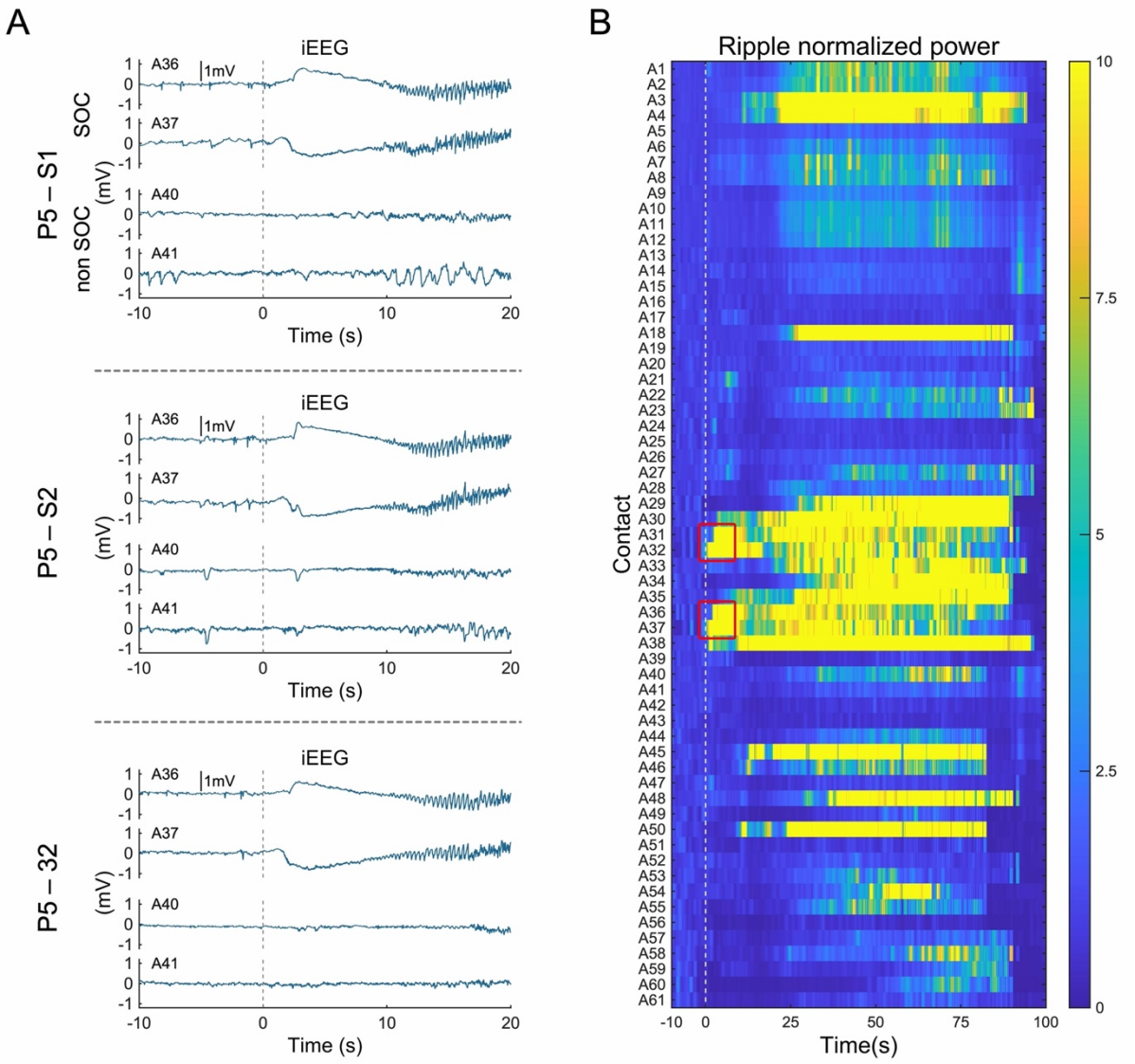


**Figure 1** Seizure onset contact (SOC) and preceding ripple contact (PRC)

Patient 5 (P5) showed three focal-to-bilateral tonic-clonic seizures (Seizure 1(S1), S2 and S3). A. Initial raw intracranial electroencephalogram (iEEG) changes included disappearance of background activities, DC shifts, and low-voltage fast waves. The contact of A31, A32, A36, and A37 (only A36 and A37 are displayed) showed the same pattern of epileptic discharges across all three seizures. We defined these four contacts as SOC, and we randomly selected one contact—A36 in this patient—for further investigations. For reference, the non SOC, A40 and A41 that showed no epileptic changes at the seizure onset (SO) were displayed. B. Ripple normalized powers are shown. Immediately after the SO, ripple normalized powers >10 were observed a cluster at A31, A32, A36, and A37 (red square). These ripple activities preceded the later ripple activities by several seconds, and we defined them as *preceding ripple activities*. Therefore, above four contacts were the PRC, and the SOC matched the PRC in P5. The 0 s corresponded to the SO. All implanted contacts are indicated on the vertical axis of B.

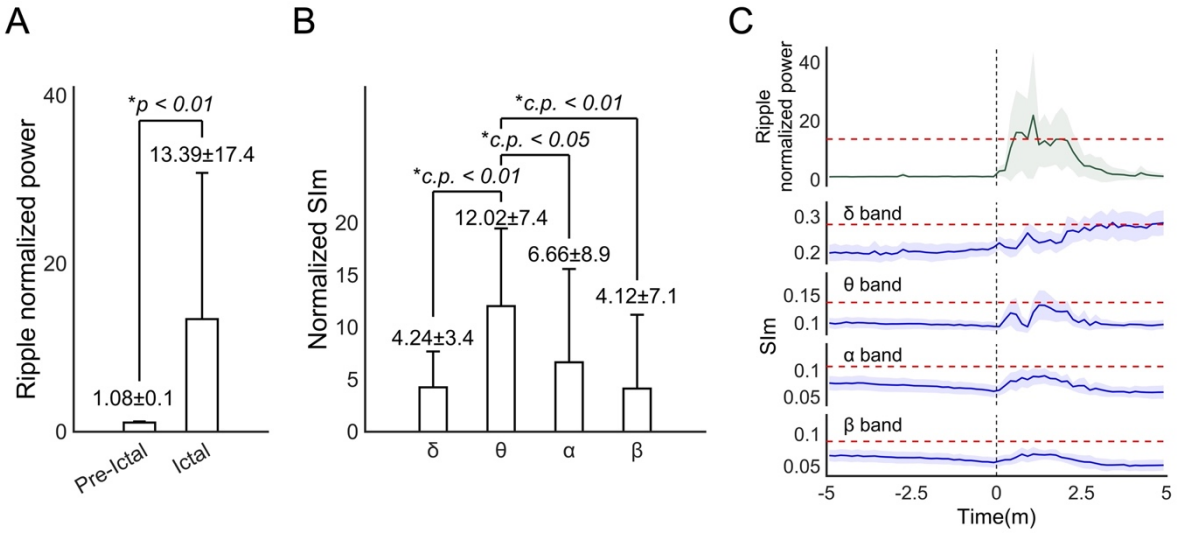


**Figure 2** Characteristics of ripple power and phase-amplitude coupling (PAC) related to seizures.

A. The ripple normalized power in ictal state was significantly greater than that in pre-ictal state. B. The normalized synchronization index magnitude (SIm) during ripple power burst related to seizures achieved the significant highest values in θ band. C. Temporal plot of ripple normalized power, θ-, α-, and β-SIm increased and achieved the peak after the seizure onset (SO) (0 min). δ-SIm achieved the peak after completion of ripple power burst. The familywise error (FWE)-corrected threshold is indicated as red dashed line.

c.p: corrected p value with Bonferroni correction. The error bars (EB) in A, and B indicate standard deviation. The EB in C indicate 95% confidence intervals.

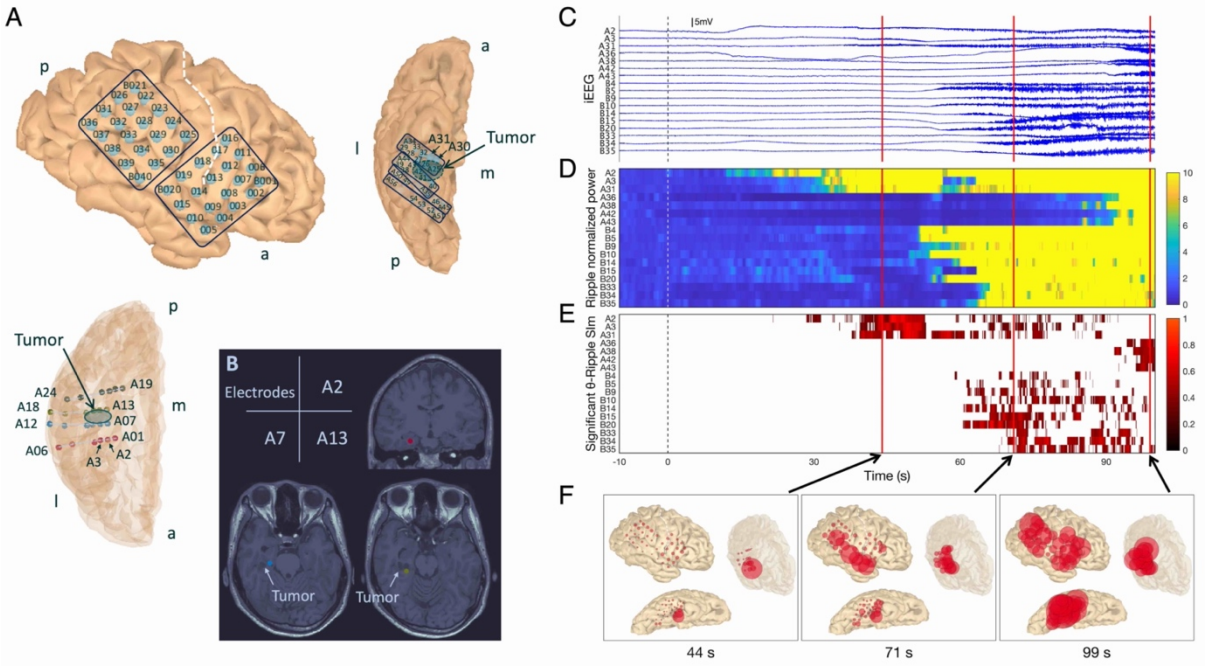


**Figure 3** Seizure profile in Patient 1 (P1)-Seizure 1 (S1).

A. Depth electrodes A1–6, A7–12, A13–18, and A19–24 were targeting the parahippocampal gyrus, the anterior region of the tumor, the posterior region of the tumor, and the lingual gyrus, respectively. a. anterior; p. posterior; m. medial; l. lateral. B. The location of A2, A7, and A13 in relation the cystic tumor is shown on the T1-weighted magnetic resonance imaging. C. Intracranial electrodes' raw signals. Initial infraslow activities were observed on A2. D. The ripple normalized power started to increase after the seizure onset (SO), from the A2 and propagated to other contacts. E. Significant θ-ripple synchronization index magnitude (SIm) shows the cluster in contacts in which ripple power increased. Here, 0 s corresponds to the SO determined visually and is indicated as dashed lines. F. Ripple power distribution map. The location of red circles corresponds to each contact's location, and those located within the semitransparent brain were depth electrode contacts. The size of red circles corresponds to ripple power. The ripple power started to increase in A2 (44 s) and propagated to other contacts on the cortex along the Sylvian fissure (71 s), and almost all other regions (99 s).

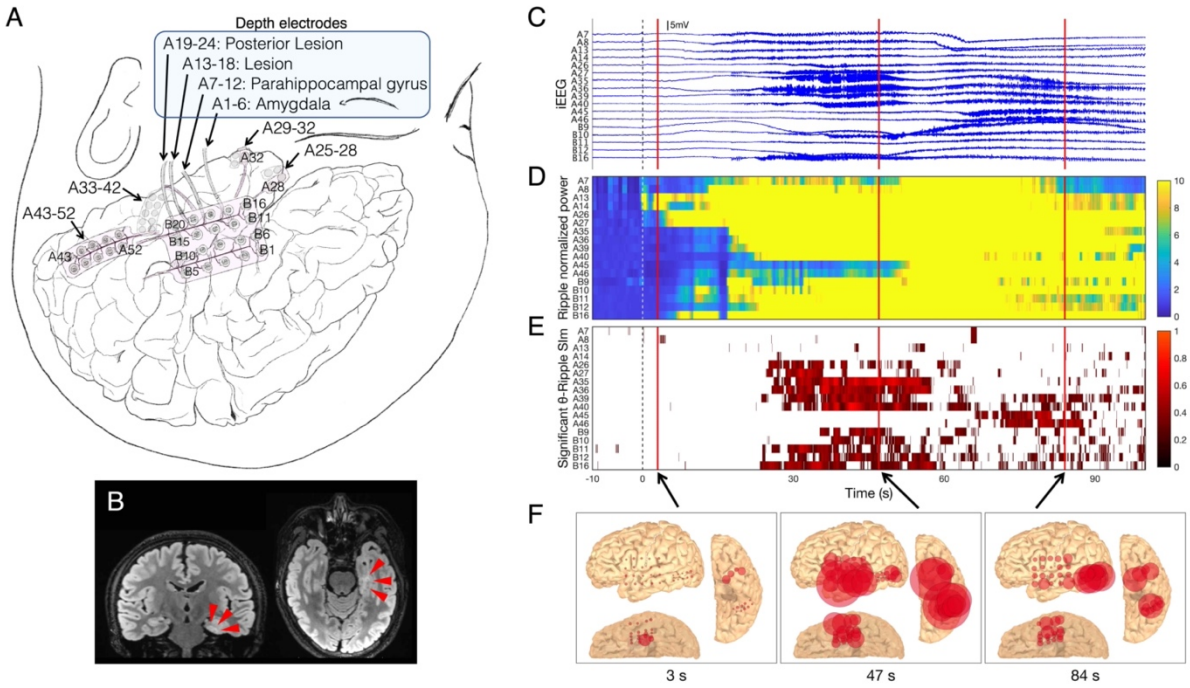


559

560 **Figure 4** Seizure profile in Patient 4 (P4)-Seizure 2 (S2).

561 A. Depth electrodes A1–24 were inserted into the left mesial temporal lobe (MTL). A13 was
562 located in the lesion. B. The high-intensity lesion in the left MTL is shown on fluid-attenuated
563 inversion recovery magnetic resonance imaging (red wedge arrows). C. In A13, initial
564 infraslow activities and low-voltage fast waves were observed. D. The ripple normalized power
565 started to increase after the seizure onset (SO), from A13 and propagated to other contacts. E.
566 Significant θ-ripple synchronization index magnitude (SIm) shows the cluster in contacts in
567 which ripple power increased. Here, 0 s corresponds to the SO determined visually and is
568 indicated as dashed lines. F. Ripple power distribution map. The location of red circles
569 corresponds to each contact's location, and those located within the semitransparent brain were
570 depth electrode contacts. The size of red circles corresponds to ripple power. The ripple power
571 started to increase in A13 (3 s) and propagated to other contacts on the cortex along the Sylvian
572 fissure (47 s), and to the posterior middle temporal gyrus (84 s).

573

574

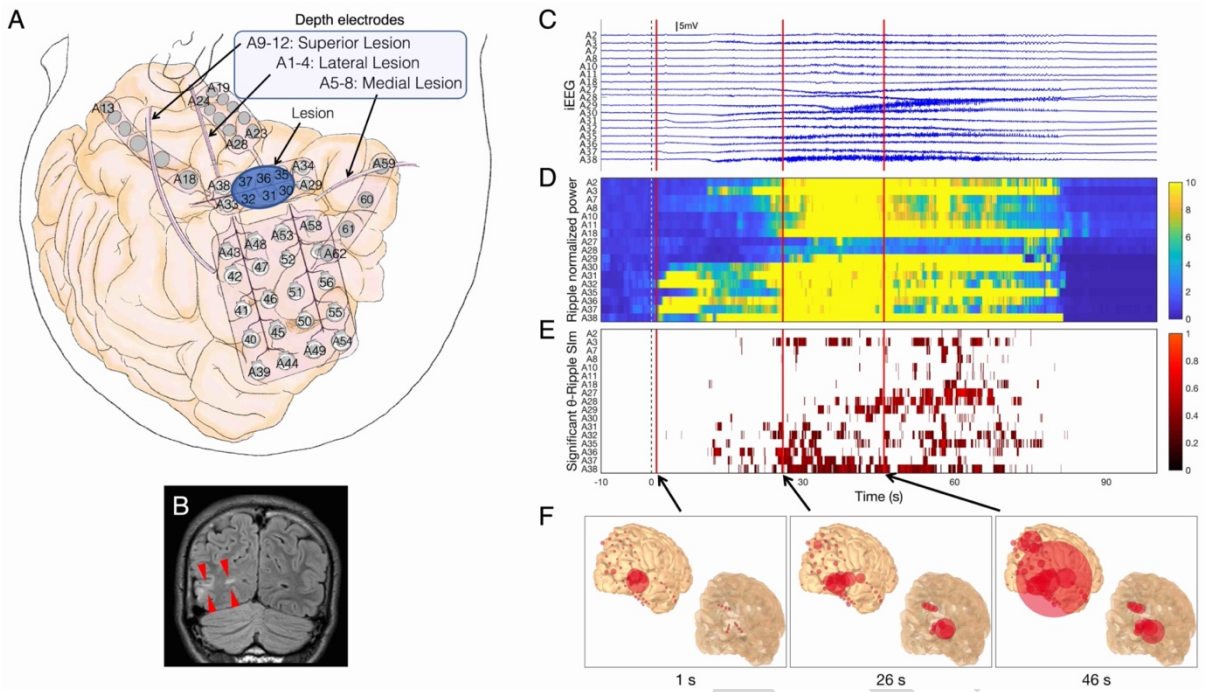


**Figure 5** Seizure profile in Patient 5 (P5)-Seizure 2 (S2).
A. Depth electrodes A1–12 were targeting around the right occipital lesion. B. The high-intensity lesion in the right occipital lobe is shown on fluid-attenuated inversion recovery magnetic resonance imaging (red wedge arrows). C. In A31, A32, A36 and A37, initial infraslow activities and low-voltage fast waves were observed. D. The ripple normalized power started to increase after the seizure onset (SO), from the A31, A32, A36 and A37 and propagated to other electrodes. E. Significant θ-ripple synchronization index magnitude (SIm) shows the cluster in contacts in which ripple power increased. Here, 0 s corresponds to the SO determined visually and is indicated as dashed lines. F. Ripple power distribution map. The location of red circles corresponds to each contact's location, and those located within the semitransparent brain were depth electrode contacts. The size of red circles corresponds to ripple power. The ripple power started to increase in A31, A32, A36 and A37 over the right occipital lesion (1 s) and propagated to the parietal lobe (46 s).

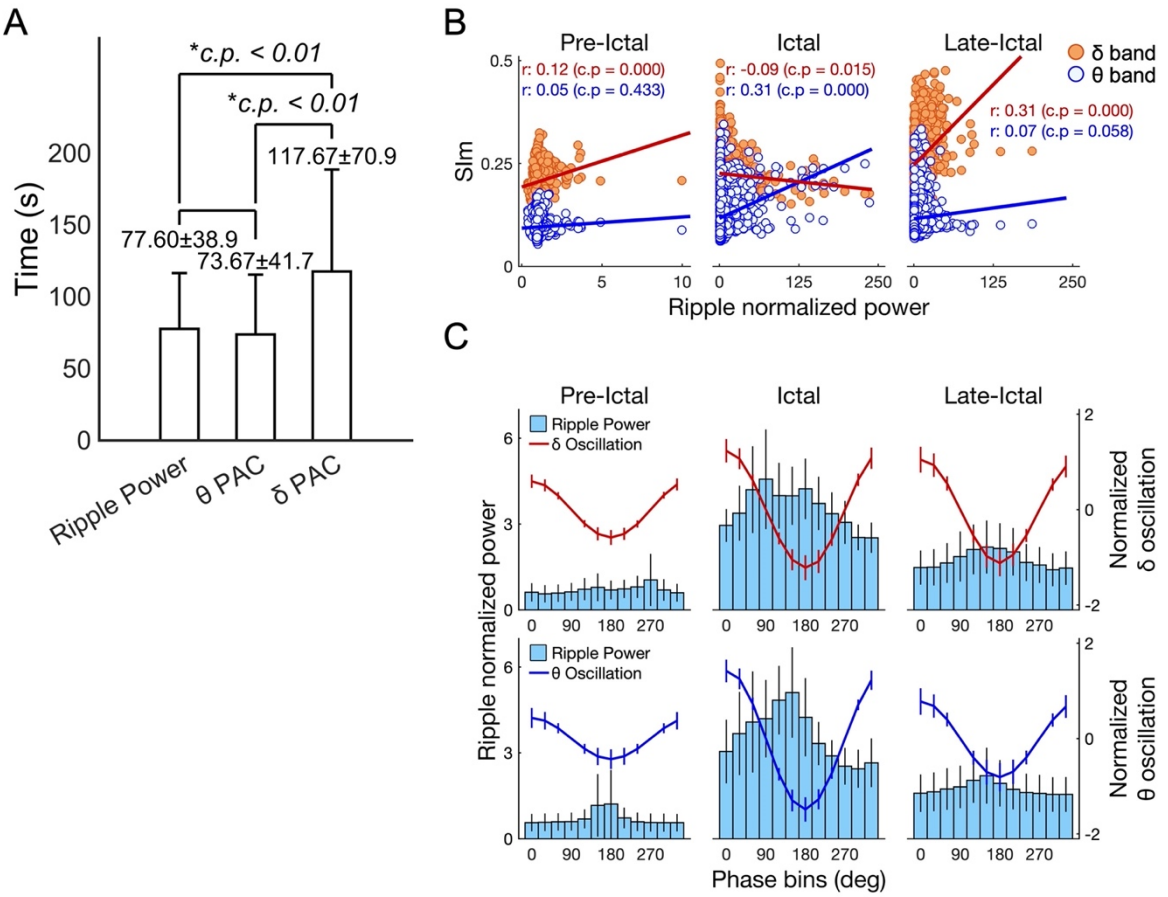


592

593 **Figure 6** Characteristics of δ- and θ-ripple phase-amplitude coupling (PAC) related to seizures.
594 A. The time taken to achieve the maximum values was compared between ripple normalized
595 power, θ-SIm (PAC), and δ-SIm (PAC). The time of δ PAC was significantly slower. B. During
596 ictal state, significant positive correlation between ripple normalized power and θ-SIm and
597 significant negative correlation between ripple normalized power and δ-SIm were observed. In
598 late-ictal state, significant positive correlation between ripple normalized power and δ-SIm was
599 observed. r: correlation coefficients, c.p: corrected p value with Bonferroni correction. C. Phase
600 tuning δ and θ oscillation showed the trough at 180°. The phase-tuning ripple normalized power
601 showed the peak at the trough with θ phase in ictal state, and with δ phase in late-ictal state.
602 The error bars (EB) in A indicate standard deviation. The EB in C indicate 95% confidence
603 intervals.

604

605

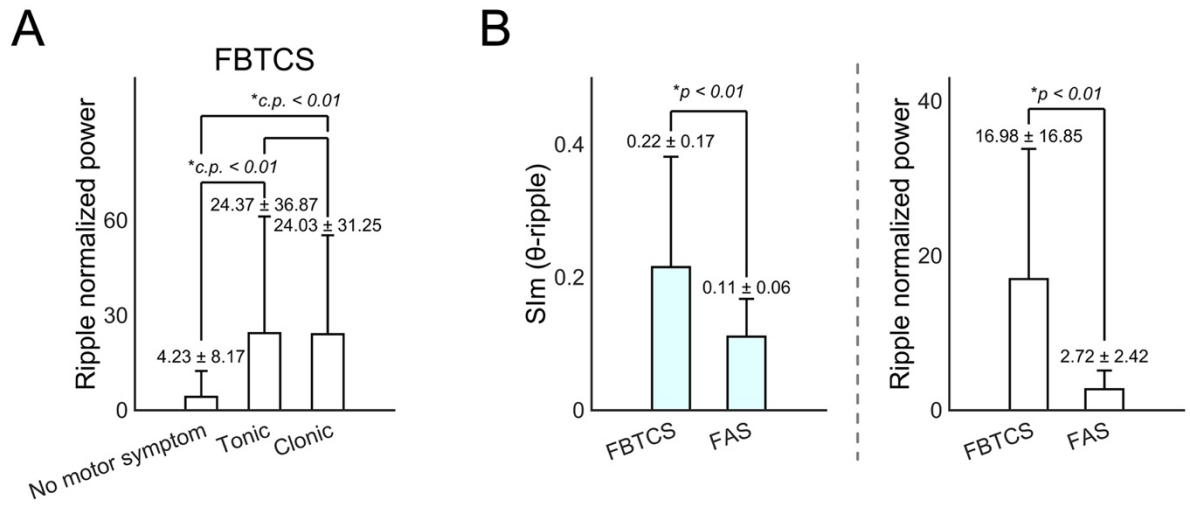


**Figure 7** Profile of focal to bilateral tonic clonic seizure (FBTCS) and focal aware seizure (FAS).

A. In FBTCS, the seizure phase changed from the no motor symptom phase, to tonic phase, and then to the clonic phase. Both the tonic and clonic phases showed significantly higher ripple normalized power—averaged from all contacts—than the no motor symptom phase. B. θ-ripple SIm and ripple normalized power obtained from seizure onset contact were compared during the no motor symptom phase between FBTCS and FAS. FBTCS showed significantly higher SIm and ripple normalized power than FAS.

c.p.: corrected p value with Bonferroni correction.

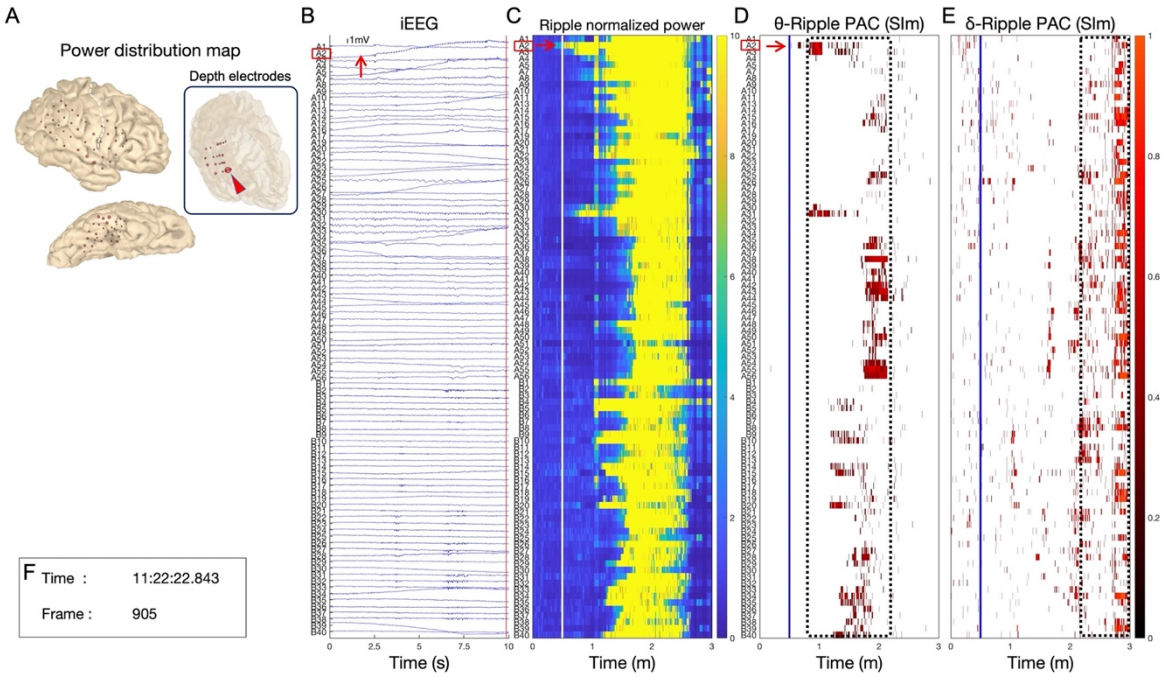


**Video 1**

Multimodal data obtained from Patient 1-Seizure 1 are shown; ripple (80–250 Hz) power distribution map (A), intracranial electroencephalograms (iEEG) signals (B), ripple normalized power (C), θ-ripple phase-amplitude coupling (PAC) (synchronization index magnitude: SIm) (D), δ-ripple PAC (SIm) (E) and time (F). The video starts 10 s before the seizure onset (SO). In power distribution map (A), red circles, corresponding to intracranial electrode contacts, were scaled linearly with ripple power changes. The circles in the semitransparent brain indicate depth electrode contacts. The rhythmic movement of red circles started from the A2 depth electrode contact (red wedge arrow), which were inserted into the right parahippocampal gyrus (A). The rhythmic fluctuations spread to the contacts over the cortex along the Sylvian fissure and that over the temporal base. The A2 contact showed initial infraslow activities (red arrow in B), followed by low-voltage fast waves, therefore we defined the A2 contact as a seizure onset contact (SOC). Ripple power increases also began from the A2 (red arrow in C), therefore in this case, a preceding ripple contact (PRC) was the A2 contact and the SOC was concordant with the PRC. SIm values scaled as black to red are statistically significant values to which the FWE-corrected threshold was applied. At ripple power increasing from the A2 contact, significant θ-ripple PAC were also observed (red arrow in D). First, significant θ-ripple PAC were observed (black bashed square in D), after that, significant δ-ripple PAC were observed (black bashed square in E). In this case, time lag between θ- and δ-ripple PAC were observed. During significantly high values of SIm, the fluctuation of red circles changed at certain rhythms. We inferred that the rhythmic fluctuations were tuned at θ or δ rhythm, and represented the PAC phenomenon. The SO is 11:22:03. The 44 s, 71 s, and 99 s in Fig. 3F correspond to 11:22:47, 11:23:14, and 11:23:42 in respectively. All implanted electrode

642 contacts after removal of noisy contacts are shown in the vertical axes (B, C, D, and E). The
643 vertical bars indicating current-time are colored red in iEEG signals (B), white in ripple
644 normalized power (C), and blue in PAC (D, and E). The vide was played at 1.5x.
645

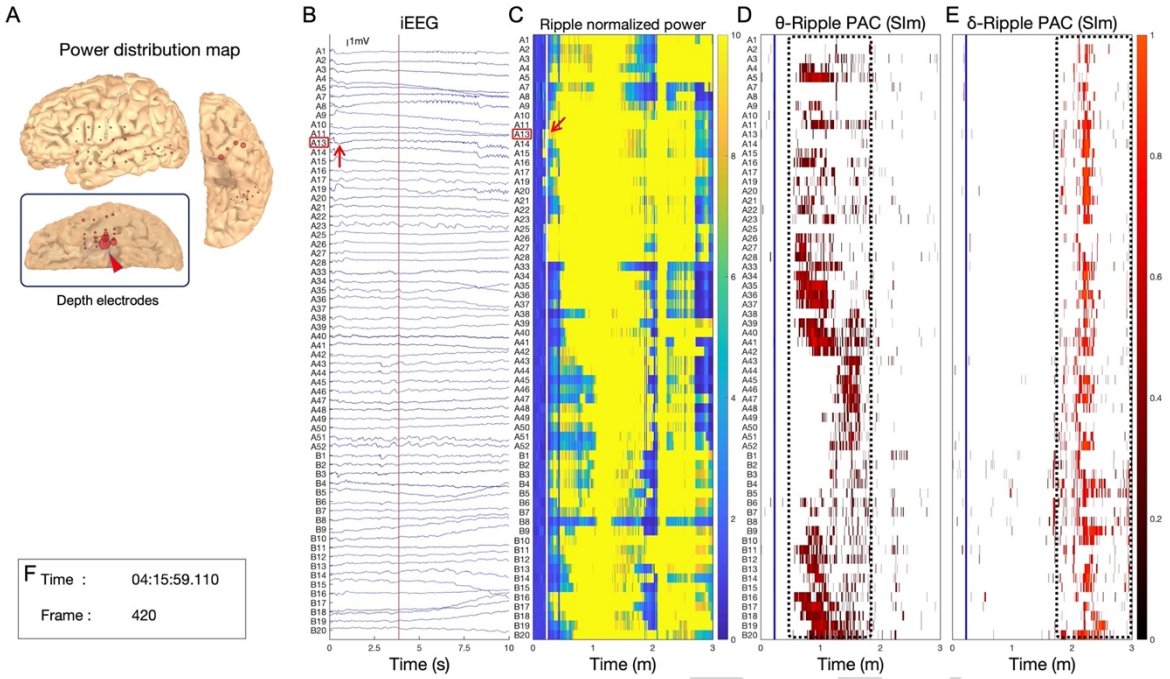


**Video 2**

Multimodal data obtained from Patient 4-Seizure 2 are shown; ripple (80–250 Hz) power distribution map (A), intracranial electroencephalograms (iEEG) signals (B), ripple normalized power (C), θ-ripple phase-amplitude coupling (PAC) (synchronization index magnitude: SIm) (D), δ-ripple PAC (SIm) (E) and time (F). The video starts 10 s before the seizure onset (SO). In power distribution map (A), red circles, corresponding to intracranial electrode contacts, were scaled linearly with ripple power changes. The circles in the semitransparent brain indicate depth electrode contacts. The rhythmic movement of red circles started from the A13 depth electrode contact (red wedge arrow), which were inserted into the left mesial temporal lobe (A). The rhythmic movement spread to the contacts over the temporal tip cortex and that over the cortex along the Sylvian fissure and that over the posterior middle temporal gyrus. The A13 contact showed initial infraslow activities (red arrow in B), followed by low-voltage fast waves, therefore we defined the A13 contact as a seizure onset contact (SOC). Ripple power increases also began from the A13 (red arrow in C), therefore in this case, a preceding ripple contact (PRC) was the A13 contact and the SOC was concordant with the PRC. SIm values scaled as black to red are statistically significant values to which the FWE-corrected threshold was applied. First, significant θ-ripple PAC were observed (black bashed square in D), after that, significant δ-ripple PAC were observed (black bashed square in E). In this case, time lag between θ- and δ-ripple PAC were observed. During significantly high values of SIm, the fluctuation of red circles changed at certain rhythms. We inferred that the rhythmic fluctuations were tuned at θ or δ rhythm, and represented the PAC phenomenon. The SO is 4:15:56. The 3 s, 47 s, and 84 s in Fig. 4F correspond to 4:15:59, 4:16:43, and 4:17:20 in respectively. All implanted electrode contacts after removal of noisy contacts are shown in the

vertical axes (B, C, D, and E). The vertical bars indicating current-time are colored red in iEEG signals (B), white in ripple normalized power (C), and blue in PAC (D, and E). The vide was played at 1.5x.

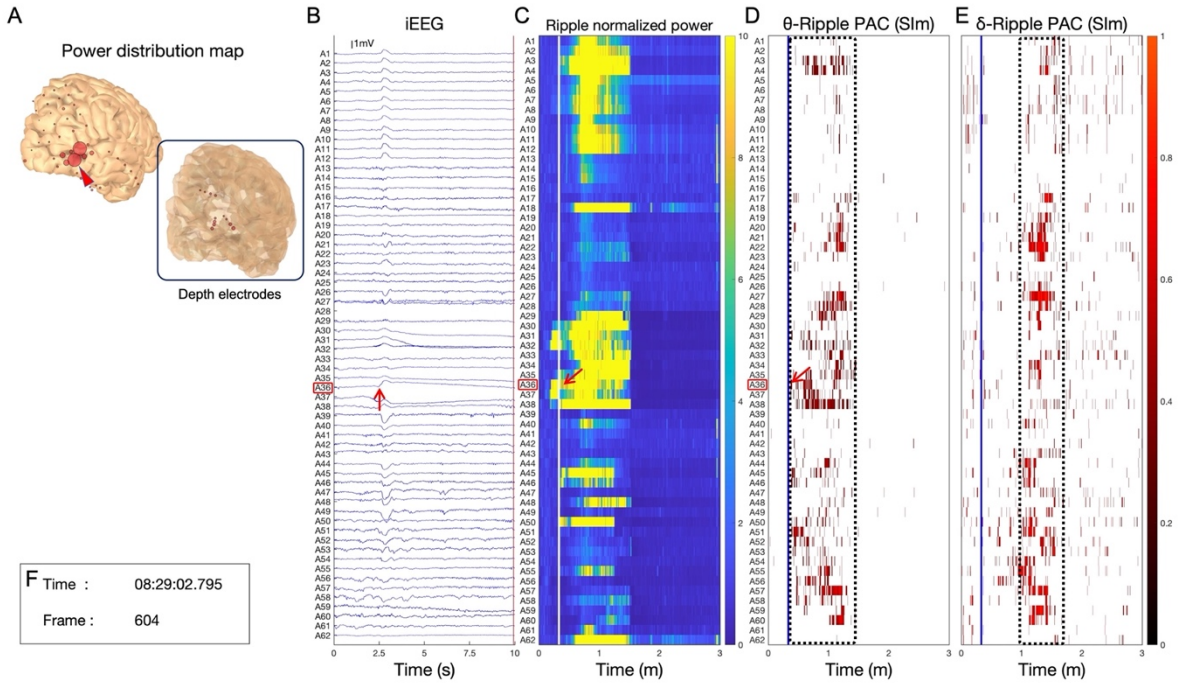


**Video 3**

Multimodal data obtained from Patient 5-Seizure 2 are shown; ripple (80–250 Hz) power distribution map (A), intracranial electroencephalograms (iEEG) signals (B), ripple normalized power (C), θ-ripple phase-amplitude coupling (PAC) (synchronization index magnitude: SIm) (D), δ-ripple PAC (SIm) (E) and time (F). The video starts 10 s before the seizure onset (SO). In power distribution map (A), red circles, corresponding to intracranial electrode contacts, were scaled linearly with ripple power changes. The circles in the semitransparent brain indicate depth electrode contacts. The rhythmic movement of red circles started from the surface electrode contacts which were placed over the right occipital lesion, including the A36 contact (red wedge arrow in A). The rhythmic movement spread to the contacts over the parietal lobe. The A36 contact showed initial infraslow activities (red arrow in B), followed by low-voltage fast waves, therefore we defined the A36 contact as a seizure onset contact (SOC). Ripple power increases also began from the A36 (red arrow in C), therefore in this case, a preceding ripple contact (PRC) was the A36 contact and the SOC was concordant with the PRC. SIm values scaled as black to red are statistically significant values to which the FWE-corrected threshold was applied. At ripple power increasing from the A36 contact, significant θ-ripple PAC were also observed (red arrow in D). First, significant θ-ripple PAC were observed (black bashed square in D), after that, significant δ-ripple PAC were observed (black bashed square in E). In this case, time lag between θ- and δ-ripple PAC were observed. During significantly high values of SIm, the fluctuation of red circles changed at certain rhythms. We inferred that the rhythmic fluctuations were tuned at θ or δ rhythm, and represented the PAC phenomenon. The SO is 8:28:53. The 1 s, 26 s, and 46 s in Fig. 5F correspond to 8:28:54, 8:29:19, and 8:29:39 in respectively. All implanted electrode contacts after removal of noisy contacts are shown in

the vertical axes (B, C, D, and E). The vertical bars indicating current-time are colored red in iEEG signals (B), white in ripple normalized power (C), and blue in PAC (D, and E). The vide was played at 1.5x.

## References


Akiyama T, Chan DW, Go CY, Ochi A, Elliott IM, Donner EJ, et al. Topographic movie of intracranial ictal high-frequency oscillations with seizure semiology: epileptic network in Jacksonian seizures. Epilepsia 2011;52(1):75-83.

Akiyama T, Otsubo H, Ochi A, Galicia EZ, Weiss SK, Donner EJ, et al. Topographic movie of ictal high-frequency oscillations on the brain surface using subdural EEG in neocortical epilepsy. Epilepsia 2006;47(11):1953-7.

Amiri M, Frauscher B, Gotman J. Phase-amplitude coupling is elevated in deep sleep and in the onset zone of focal epileptic seizures. Front Hum Neurosci 2016;10:387.

Amiri M, Frauscher B, Gotman J. Interictal coupling of HFO s and slow oscillations predicts the seizure‐onset pattern in mesiotemporal lobe epilepsy. Epilepsia 2019;60(6):1160-70.

Ayoubian L, Lacoma H, Gotman J. Automatic seizure detection in SEEG using high frequency activities in wavelet domain. Med Eng Phys 2013;35(3):319-28.

Canolty RT, Edwards E, Dalal SS, Soltani M, Nagarajan SS, Kirsch HE, et al. High gamma power is phase-locked to theta oscillations in human neocortex. Science 2006;313(5793):1626-8.

Cohen MX. Assessing transient cross-frequency coupling in EEG data. J Neurosci Methods 2008;168(2):494-9.

Cohen MX. Analyzing neural time series data: theory and practice: MIT press, 2014.

Dichter MA. Basic mechanisms of epilepsy: targets for therapeutic intervention. Epilepsia 1997;38:S2-S6.

Edakawa K, Yanagisawa T, Kishima H, Fukuma R, Oshino S, Khoo HM, et al. Detection of Epileptic Seizures Using Phase-Amplitude Coupling in Intracranial Electroencephalography. Sci Rep 2016;6.

Haegens S, Nácher V, Luna R, Romo R, Jensen OJPotNAoS. α-Oscillations in the monkey sensorimotor network influence discrimination performance by rhythmical inhibition of neuronal spiking. 2011;108(48):19377-82.

Hashimoto H, Hasegawa Y, Araki T, Sugata H, Yanagisawa T, Yorifuji S, et al. Non-invasive detection of language-related prefrontal high gamma band activity with beamforming MEG. Sci Rep 2017;7(1):14262.

Hashimoto H, Kameda S, Maezawa H, Oshino S, Tani N, Khoo HM, et al. A Swallowing Decoder Based on Deep Transfer Learning: AlexNet Classification of the Intracranial Electrocorticogram. Int J Neural Syst;0(0):2050056.

Hashimoto H, Khoo HM, Yanagisawa T, Tani N, Oshino S, Kishima H, et al. Coupling between infraslow activities and high-frequency oscillations precedes seizure onset. Epilepsia Open 2020a;5(3):501-6.

Hashimoto H, Takahashi K, Kameda S, Yoshida F, Maezawa H, Oshino S, et al. Swallowing-

related neural oscillation: An intracranial EEG study. bioRxiv 2020b.
Ibrahim GM, Wong SM, Anderson RA, Singh-Cadieux G, Akiyama T, Ochi A, et al. Dynamic modulation of epileptic high frequency oscillations by the phase of slower cortical rhythms. Exp Neurol 2014;251:30-8.
Iimura Y, Jones K, Takada L, Shimizu I, Koyama M, Hattori K, et al. Strong coupling between slow oscillations and wide fast ripples in children with epileptic spasms: Investigation of modulation index and occurrence rate. Epilepsia 2018;59(3):544-54.
Ikeda A, Taki W, Kunieda T, Terada K, Mikuni N, Nagamine T, et al. Focal ictal direct current shifts in humanepilepsy as studied by subdural and scalp recording. Brain 1999;122(5):827-38.
Ikeda A, Terada K, Mikuni N, Burgess RC, Comair Y, Taki W, et al. Subdural recording of ictal DC shifts in neocortical seizures in humans. Epilepsia 1996;37(7):662-74.
Imamura H, Matsumoto R, Inouchi M, Matsuhashi M, Mikuni N, Takahashi R, et al. Ictal wideband ECoG: direct comparison between ictal slow shifts and high frequency oscillations. Clin Neurophysiol 2011;122(8):1500-4.
Jirsch J, Urrestarazu E, LeVan P, Olivier A, Dubeau F, Gotman J. High-frequency oscillations during human focal seizures. Brain 2006;129(6):1593-608.
Kanazawa K, Matsumoto R, Imamura H, Matsuhashi M, Kikuchi T, Kunieda T, et al. Intracranially recorded ictal direct current shifts may precede high frequency oscillations in human epilepsy. Clin Neurophysiol 2015;126(1):47-59.
Kitchigina VF, Butuzova MV. Theta activity of septal neurons during different epileptic phases: the same frequency but different significance? Exp Neurol 2009;216(2):449-58.
Luo H, Poeppel DJN. Phase patterns of neuronal responses reliably discriminate speech in human auditory cortex. Neuron 2007;54(6):1001-10.
Maris E, Oostenveld R. Nonparametric statistical testing of EEG- and MEG-data. J Neurosci Methods 2007;164(1):177-90.
Modur PN, Zhang S, Vitaz TW. Ictal high‐frequency oscillations in neocortical epilepsy: implications for seizure localization and surgical resection. Epilepsia 2011;52(10):1792-801.
Nariai H, Matsuzaki N, Juhász C, Nagasawa T, Sood S, Chugani HT, et al. Ictal high‐frequency oscillations at 80–200 Hz coupled with delta phase in epileptic spasms. Epilepsia 2011;52(10):e130-e4.
Nonoda Y, Miyakoshi M, Ojeda A, Makeig S, Juhasz C, Sood S, et al. Interictal high-frequency oscillations generated by seizure onset and eloquent areas may be differentially coupled with different slow waves. Clin Neurophysiol 2016;127(6):2489-99.
Ochi A, Otsubo H, Donner EJ, Elliott I, Iwata R, Funaki T, et al. Dynamic changes of ictal high-frequency oscillations in neocortical epilepsy: using multiple band frequency analysis. Epilepsia 2007;48(2):286-96.
Perucca P, Dubeau F, Gotman J. Intracranial electroencephalographic seizure-onset patterns: effect of underlying pathology. Brain 2014;137(Pt 1):183-96.

779 Ray S, Crone NE, Niebur E, Franaszczuk PJ, Hsiao SS. Neural correlates of high-gamma
780 oscillations (60–200 Hz) in macaque local field potentials and their potential implications in
781 electrocorticography. J Neurosci 2008;28(45):11526-36.
782 Rodin E, Modur P. Ictal intracranial infraslow EEG activity. Clin Neurophysiol
783 2008;119(10):2188-200.
784 Schönberger J, Birk N, Lachner‐Piza D, Dümpelmann M, Schulze‐Bonhage A, Jacobs J.
785 High‐frequency oscillations mirror severity of human temporal lobe seizures. Annals of
786 Clinical and Translational Neurology 2019;6(12):2479-88.
787 So N, Gotman J. Changes in seizure activity following anticonvulsant drug withdrawal.
788 Neurology 1990;40(3 Part 1):407-.
789 Wang S, Wang IZ, Bulacio JC, Mosher JC, Gonzalez‐Martinez J, Alexopoulos AV, et al.
790 Ripple classification helps to localize the seizure‐onset zone in neocortical epilepsy. Epilepsia
791 2013;54(2):370-6.
792 Weiss SA, Orosz I, Salamon N, Moy S, Wei L, Van't Klooster MA, et al. Ripples on spikes
793 show increased phase‐amplitude coupling in mesial temporal lobe epilepsy seizure‐onset
794 zones. Epilepsia 2016;57(11):1916-30.
795 Wu S, Kunhi Veedu HP, Lhatoo SD, Koubeissi MZ, Miller JP, Lüders HO. Role of ictal baseline
796 shifts and ictal high‐frequency oscillations in stereo‐electroencephalography analysis of
797 mesial temporal lobe seizures. Epilepsia 2014;55(5):690-8.
798 Yanagisawa T, Yamashita O, Hirata M, Kishima H, Saitoh Y, Goto T, et al. Regulation of Motor
799 Representation by Phase-Amplitude Coupling in the Sensorimotor Cortex. J Neurosci
800 2012;32(44):15467-75.
801 Zijlmans M, Jiruska P, Zelmann R, Leijten FS, Jefferys JG, Gotman J. High‐frequency
802 oscillations as a new biomarker in epilepsy. Ann Neurol 2012;71(2):169-78.
803

**Phase-amplitude coupling of ripple activities during seizure evolution with theta phase**

Hiroaki Hashimoto. M.D., Ph.D.[1,2,3]*, Hui Ming Khoo. M.D., Ph.D.[4], Takufumi Yanagisawa. M.D., Ph.D.[4], Naoki Tani. M.D., Ph.D.[4], Satoru Oshino. M.D., Ph.D.[4], Haruhiko Kishima. M.D., Ph.D.[4], Masayuki Hirata. M.D., Ph.D.[1,3,4]

[1] Department of Neurological Diagnosis and Restoration, Graduate School of Medicine, Osaka University, Suita 565-0871, Japan
[2] Department of Neurosurgery, Otemae Hospital, Osaka, 540-0008, Japan
[3] Endowed Research Department of Clinical Neuroengineering, Global Center for Medical Engineering and Informatics, Osaka University, Suita 565-0871, Japan
[4] Department of Neurosurgery, Graduate School of Medicine, Osaka University, Suita 565-0871, Japan

*** Correspondence:**
Hiroaki Hashimoto, M.D., Ph.D.
Invited Researcher, Department of Neurological Diagnosis and Restoration, Graduate School of Medicine, Osaka University, Yamadaoka 2-2, Suita, Osaka, Japan
Tel.: +81-6-6210-8429
Fax: +81-6-6210-8430
E-mail: h-hashimoto@ndr.med.osaka-u.ac.jp



Supplementary Figure 1

**Supplementary Figure 1** Normalized power of the low frequency bands at the pre-ictal and ictal states.

The main low frequency band, coupled with ripple, was the δ band in 2/15 seizures (13%), θ band in 12/15 seizures (80%), and α band in 1/15 seizures (7%) (Table 1). For each seizure group with a different low frequency band (δ-ripple coupling in A, θ-ripple coupling in B, and α-ripple coupling in C), we compared the low frequency normalized power at the δ, θ, α, and β bands during the pre-ictal and ictal states using the Kruskal-Wallis test with Bonferroni correction. Except for the pre-ictal state of δ-ripple coupling, there were significant differences (corrected *p* values (c.p) < 0.05). In all three groups, during the pre-ictal state, the δ band tended to achieve the more values than others, however, during the ictal state, β band tended to achieve greater values than others. The main low frequency band that shows coupling with ripple doesn't match the low frequency band that shows power increasing.